

Polymer Chemistry

Accepted Manuscript



This is an *Accepted Manuscript*, which has been through the Royal Society of Chemistry peer review process and has been accepted for publication.

Accepted Manuscripts are published online shortly after acceptance, before technical editing, formatting and proof reading. Using this free service, authors can make their results available to the community, in citable form, before we publish the edited article. We will replace this *Accepted Manuscript* with the edited and formatted *Advance Article* as soon as it is available.

You can find more information about *Accepted Manuscripts* in the [Information for Authors](#).

Please note that technical editing may introduce minor changes to the text and/or graphics, which may alter content. The journal's standard [Terms & Conditions](#) and the [Ethical guidelines](#) still apply. In no event shall the Royal Society of Chemistry be held responsible for any errors or omissions in this *Accepted Manuscript* or any consequences arising from the use of any information it contains.

**Enhanced Performance of Fluorinated Quinoxaline-Containing
Polymers by Replacing Carbon with Silicon Bridging Atoms on
Dithiophene Donor Skeleton**

Xiaopeng Xu, Kai Li, Zuojia Li, Ying Li,* Zhenguo Wang, Qiang Peng*

Key Laboratory of Green Chemistry and Technology of Ministry of Education, College of
Chemistry, and State Key Laboratory of Polymer Materials Engineering, Sichuan University,
Chengdu 610064, P. R. China

*To whom correspondence should be addressed: Tel: +86-28-86510868; fax: +86-28-86510868;

e-mail: qiangpengjohnny@yahoo.com

Abstract:

Fluorinated quinoxaline unit is an attractive acceptor block to building low band gap photovoltaic polymers. In this contribution, two novel fluorinated quinoxaline-based copolymers, **PCPDTBFQ** and **PDTSBFQ**, have been successfully synthesized by combination of cyclopentadithiophene (CPDT) or dithienosilole (DTS) donor blocks in the polymeric backbones. The bridging atom effect shows great influence on the absorption property, energy level, carrier mobility as well as photovoltaic performance. **PDTSBFQ** with Si bridging atom shows a little blue-shift in the UV-vis absorption, and a little larger band gap than those of **PCPDTBFQ**. However, **PDTSBFQ** shows a stronger aggregation even in solution state. Compared with carbon, silica atom afforded **PDTSBFQ** with a lower-lying HOMO level, expecting to have a high V_{oc} of its polymer solar cells (PSCs). **PDTSBFQ** also exhibits a better crystallinity and a molecular ordering property than **PCPDTBFQ** from the XRD study. The hole-only device based on **PDTSBFQ** exhibited a higher hole mobility of $1.5 \times 10^{-5} \text{ cm}^2 \text{ V}^{-1} \text{ s}^{-1}$ than that of $4.1 \times 10^{-6} \text{ cm}^2 \text{ V}^{-1} \text{ s}^{-1}$ for **PCPDTBFQ**. Conventional PSCs were fabricated to investigate the bridging atom effect on the photovoltaic properties of these two copolymers. Different interfacial layer (IFL) of Ca and PFN had been tried to optimize the performance of the fabricated PSCs. When using a Ca/Al top electrode, **PCPDTBFQ** and **PDTSBFQ** devices showed PCEs of 2.16% and 4.43%, respectively. The better performance of **PDTSBFQ** device would thank for the improvements of its V_{oc} , J_{sc} and FF values just by choose of silica bridging atoms. After replacing the Ca/Al with a PFN/Al cathode, the performance of both

PCPDTBFQ and **PDTSBFQ** devices was enhanced largely. **PDTSBFQ** device achieved the highest PCE of 5.92% with a V_{oc} of 0.77 V, a J_{sc} of 12.25 mA cm⁻² and an FF of 0.63. The primary results gave a simple but efficient strategy to design high performance dithiophene-quinoxaline polymer donors for organic solar cell applications.

Keywords:

Polymer solar cells, Bridging atom effect, Fluorinated quinoxaline, Cyclopentadithiophene, Dithienosilole

Introduction

Polymer solar cells (PSCs) have been achieving considerable interest due to many advantages, including the thin-film architecture and low material consumption resulting from a high absorption coefficient, efficient wet-process, and low manufacturing energy requirement. Meanwhile, their low specific weight, mechanical flexibility, tunable material properties, and high transparency make them possess vast potential applications for future development.¹ Bulk-heterojunction (BHJ) device, which involves an interpenetrating network of electron donor (conjugated polymers) and acceptor materials (fullerene derivatives) in the active layer, is known as one of the most efficient type of PSCs for satisfied addressing the issue of exciton disassociation.^{1a,2} With so many kind of good materials and wonderful process techniques being discovered and developed for the past two decades, the improvements in device performance have been driven to achieve a high power conversion efficiency (PCE) over 9%.³

In search for high performance PSCs, the design and synthesis of new π -conjugated organic semiconductors has been a hot topic of great research interests for the past few years.⁴ From the view point of π -conjugated polymer designation, the donor-acceptor (D-A) alternating motif, combining electron-rich (donor) and electron-deficient (acceptor) subunits, is considered to be a well established approach to attain a high efficiency.⁵ By developing different donor and/or acceptor units and incorporating them with rational counterparts, the optical absorption property and band gap could be finely tuned, resulting from the different inter- or intramolecular

charge (ICT) and π - π^* transition processes.⁶ Among of them, the low band gap (LBG) copolymer may be the most successful candidate, aiming at achieving broad absorption, high hole mobility, and suitable energy level.^{2b,6a,7} However, low band gap does not necessarily guarantee high performance. Many copolymers feature low band gaps, but the relative narrow range of solar spectrum absorption limits their performance. The tandem device architecture can provide an effective way to solve above problem, which employs two or more semiconductors with different band gaps enabling absorption over a broad range of photon energies.^{2b,3b,8} But more combined active layers involve more complex processing procedures, which requires more advanced technical supports and increases the overall fabrication costs. Furthermore, lowering the band gap may cause a rising of highest occupied molecular orbital (HOMO) level, resulting in a low open circuit voltage (V_{oc}) in PSCs.⁹ In this regard, a “weak donor-strong acceptor” strategy was proposed to simultaneously lower the HOMO energy level and keep the low band gap, as required by the ideal polymer donors.¹⁰ A series of such materials have been successfully demonstrated with high efficiency in typical BHJ devices.^{3c,4b,7,11} Up to date, the PCEs for single junction BHJ devices based on LBG copolymers have already broken the 9% milestone.^{3c,12}

Quinoxaline (Q_x) skeleton has been extensively studied in recent years as a strong electron deficient unit for building high performance LBG copolymers.¹³ In addition, the incorporation of electron withdrawing fluorine atom onto the Q_x moiety has become more and more attractive.^[14] Because of many unique characteristics, such as the most electronegative element, the smallest electron-withdrawing group, a great

influence on inter- and/or intramolecular interactions through secondary bonds,^{11c} fluorinated conjugated polymers and their devices exhibit improved thermal and oxidative stability, elevated resistance to degradation.¹⁵ More important than that, the V_{oc} , short circuit density (J_{sc}) and fill factor (FF) as well as PCE, can be simultaneously improved.^{14a,16} Our previous work focused on benzodithiophene (BDT) and fluorinated Q_x copolymers has demonstrated a good example for efficient tuning the thermal stability, absorption range, energy level, charge transport, and photovoltaic properties by side chain engineering of both branching degree and dimensionality.¹⁷ To achieve higher performance, other good donor blocks should be tried to balance and optimize the relationship between the molecular structure and the photovoltaic properties. On the other hand, cyclopentadithiophene (CPDT) and dithienosilole (DTS) are typical weak donor units, which have been used for constructing efficient LBG photovoltaic materials. Polymers based on these two blocks exhibit good solubility and thermal property, good crystallinity, excellent morphology and high efficiency.^{11b,11d,18} Furthermore, they are also endowed with larger optical absorption coefficient than BDT counterparts.^{18d,19} It is expected that CPDT and DTS based polymers can obtain more satisfied performance when copolymerized with fluorinated Q_x . However, only a few CPDT- Q_x and DTS- Q_x copolymers have been reported, letting alone the fluorinated Q_x block.²⁰

Based on above considerations, we report here the synthesis and characterization of two novel fluorinated Q_x based copolymers, **PCPDTBFQ** and **PDTSBFQ** (Scheme 1), in which two different weak donor units of CPDT and DTS with similar

π -conjugated backbones have been incorporated in the main chains. By taking advantage of the “weak donor-strong acceptor” strategy and the benefits of fluorine atom, an improvement of device performance would be expected in such D-A system. The bridging atom effect was also investigated in detail on the optical and photovoltaic properties. Replacing the bridging carbon atom by a silicon atom, **PDTSBFQ** exhibits the higher thermal stability, more ordered molecular organization, and more superior nanoscale phase splitting structure when blended with [6,6]-phenyl-C₇₁-butyric acid methyl ester (PC₇₁BM). A high PCE of 5.92% was obtained from **PDTSBFQ** device in a conventional structure.

Results and discussion

Synthesis and characterization

The synthetic routes of the copolymers are shown in Schemes 2. The **BFQ** and organic tin monomers were synthesized according to previously reported procedures.^{17,21} **PCPDTBFQ** and **PDTSBFQ** were then prepared through Stille-coupling polymerization in good yields, using Pd₂(dba)₃/P(*o*-tolyl)₃ as a catalyst system. The crude polymers were precipitated into methanol and filtered, followed by sequential Soxhlet extraction with methanol, hexane and chloroform to remove byproducts and oligomers. The purified copolymers were obtained and collected from the chloroform fraction by precipitation into methanol again. The chemical structures of target copolymers were confirmed by ¹H NMR spectroscopy and elemental analysis. The two polymers exhibit an excellent film-casting property and good solubility in some common organic solvents, such as chloroform, tetrahydrofuran,

chlorobenzene, dichlorobenzene. The number-average molecular weights (M_n) and polydispersity indices (PDI) of the two polymers were measured at 35 °C by gel permeation chromatography (GPC) using THF as the eluent and polystyrene as the internal standard. The M_n values of **PCPDTBFQ** and **PDTSBFQ** were determined to be 16.0 and 34.1 kDa, respectively. The PDI of **PCPDTBFQ** is 2.2. But for **PDTSBFQ**, the PDI is relative high up to 6.5, which might be overestimated because of the strong aggregation property of **PDTSBFQ** in organic solution even at room temperature.^{21e,22} In order to confirm this speculation, the molecular weights were further measured using high temperature GPC. The M_n of **PDTSBFQ** was determined at 80 °C to be about 13.6 kDa with a relatively narrow PDI of 2.7. The aggregation phenomenon could be also confirmed by the UV-vis spectra (*vide infra*).

The thermal property of conjugated polymers plays a very important role in PSCs. The thermal stability was investigated with thermogravimetric analysis (TGA). As shown in Fig. 1a, the degradation temperatures (T_d) of **PCPDTBFQ**, and **PDTSBFQ** with 5% weight loss were measured to be about 421 and 430 °C, respectively. Using Si bridging atom can improve the thermal stability of these fluorinated Q_x based copolymers, which is beneficial for its device fabrication and evaluation. On the other hand, no endo- or exothermal signals were observed from differential scanning calorimetry (DSC) measurements in the range of 0-230 °C from the second heating run (Fig. 1b), implying that these two polymers are thermally robust. The results of molecular weights and the thermal analysis are listed in Table 1.

Optical properties

The UV-vis absorption properties of these two polymers were measured in solutions and thin solid films. We first investigated the UV-vis absorption in chloroform solution with a concentration of 10^{-5} M. As shown in Fig. 2a, it's interesting to find that **PDTSBFQ** shows a slightly red-shift than that of **PCPDTBFQ** in solution. This is likely ascribed to the strong aggregation of **PDTSBFQ** in solution. To verify this assumption, we diluted the polymer solution to a small concentration of 10^{-6} M. By this treatment, the absorption of **PDTSBFQ** was blue-shifted distinctly with about 8 nm of maximum absorption peak. When this solution was heated to 60 °C, this shift became larger to about 25 nm (Fig. 2b). However, when adopting the same conditions, the maximum absorption peaks were almost steadfast for **PCPDTBFQ**, with only a little blue shift of the maximum peak and the edge absorption during dilute and heat processes. The film absorption profile of **PDTSBFQ** shows more multiple well defined transitions, whereas that of **PCPDTBFQ** remains broad. A plausible explanation for that may be greater molecular order in **PDTSBFQ** backbones, which leads to better interchromophore electronic coupling. This is consistent with previous literature findings where polymers containing Si bridged DTS possess a higher degree of solid-state crystallinity compared to C bridged CPDT.^{18c,18d,23,24} The result will be confirmed by the X-ray diffraction (XRD) profile measurements (*vide infra*). Compared them to the BDT based polymers,¹⁷ the remarkable red-shift makes them have narrower band gaps, which can be expected to induce an elevation of the short circuit current density (J_{sc}) of their PSCs. Both **PCPDTBFQ** and **PDTSBFQ** showed a strong ICT transition absorption peak in the region of 500 to 700 nm, and their

optical energy band gaps (E_g^{opt}) could be calculated to be 1.60 eV and 1.63 eV, respectively (Table 2). To further investigate the concentration and temperature effects on the intermolecular interactions of these two polymers, we normalized the absorption data by the highest electronic vibration energy peaks (Fig. 2c and 2d). It's interesting to note that the two polymers behave an absolutely different variation tendency. When the solution was diluted and heated, the solution maximum absorption peak of **PDTSBFQ** blue-shifted and the intensity declined in the meantime, which is attributed to breakup of the intrachain aggregates.^{18b,25} However, no distinct change was found for **PCPDTBFQ** with the same treatments, which signified an insusceptible intramolecular interactions in which the molecular structure of the backbone governed the optical features.^{18b} The strong and impressionable intramolecular interactions of **PDTSBFQ** make it possible for us to do more post-optimizations, which would favor its high performance in photovoltaic applications.

Electrochemical properties

The energy levels are crucial for the selection of appropriate acceptors in BHJ PSCs.²⁶ The HOMO and LUMO levels of the copolymers were measured by cyclic voltammetry (CV) of their thin films. CV measurements were carried out on a CHI660 potentiostat/galvanostat electrochemical work station at a scan rate of 50 mV s⁻¹, with a platinum wire counter electrode and an Ag/AgCl reference electrode in a 0.1 mol L⁻¹ solution of Bu₄NClO₄ in anhydrous and nitrogen-saturated CH₃CN. A platinum plate coated with a thin film of the studied copolymers was used as the

working electrode. The energy level of the Ag/AgCl reference electrode was calibrated against the ferrocene/ferrocenium (Fc/Fc⁺) system to be 4.34 eV in this work.²⁷ As shown in Fig. 3a, both polymers exhibited reversible oxidation and reduction waves, implying their good abilities in transporting positive and negative charges.²⁸ From the onset potentials, the HOMO and LUMO energy levels were estimated to be -5.08 and -3.35 eV for **PCPDTBFQ**, -5.18 and -3.31 eV for **PDTSBFQ**, respectively. The electrochemical band gaps are then calculated to be 1.73 and 1.87 eV for **PCPDTBFQ** and **PDTSBFQ**, respectively. The difference between the optical and electrochemical band gaps could be explained by the exciton binding energy of the copolymers and/or the interfacial barriers for charge injection.²⁹ Compared to the BDT counterparts,¹⁷ the two polymers show significant reduction of LUMO with slightly increasing HOMO levels. **PDTSBQ** has almost the same HOMO level with **PBDTAB-BFQ** with BDT blocks in our previous work.¹⁷ It is well known that V_{oc} is directly proportional to the difference between HOMO energy level of a polymer donor and LUMO energy level of a fullerene derivative.³⁰ Therefore, replacing the BDT units with DTS lowers the band gap but maintains deep-lying HOMO level, giving rise to an enhancement of the overall device performance.³¹ To make a clear comparison, the electronic energy level diagrams of the polymers and PC₇₁BM are described in Fig. 3b. The LUMO gaps of 0.65-0.69 eV and HOMO gaps of 1.08-1.18 eV between the polymers and PC₇₁BM should provide a sufficient driving force to guarantee efficient exciton dissociation at the D-A interface, which would ensure energetically favorable electron transfer.³²

Theoretical calculations

To evaluate the bridging atom effect of the donor skeletons on the molecular architectures and electronic properties of the resulting polymers, DFT calculations were performed to verify stationary points as stable states for the optimized conformations and single-point energies, at the B3LYP/6-31G(d) level.^{14b,15,33} Three repeating units of the copolymers were studied as the model compounds for simulations of **PCPDTBFQ** and **PDTSBFQ**. To simplify the calculations, long alkyl chains were replaced by methyl group because they did not significantly affect the equilibrium geometries and electronic properties.^{14b,15,33} The HOMO and LUMO wave functions of the model compounds are shown in Fig. 4. It can be seen clearly from the optimized molecular backbone that Si bridged trimer adopts a more linear geometry, while it is more twist for C bridged trimer, which is also different from zigzag geometry for BDT incorporated trimers.^{17,34} The linear molecular chain of **PDTSBFQ** is in favor of more ordered organization and higher degree of crystallinity. The HOMOs feature extended delocalization along the entire conjugated backbones. The electron density mainly distributes in the middle part of the conjugated molecular skeleton, which is affected by both the donor and acceptor units. However, the LUMOs are mainly focused on the Q_x skeletons, resulting from the effect of the acceptor units. Compared with the HOMO and LUMO, the HOMO-1 and LUMO+1 seem to be distributed from the middle part to two side parts, which indicates that the internal charge transfers are possible in these conjugated systems. Thus, low band gaps of **PCPDTBFQ** and **PDTSBFQ** can be obtained by the efficient internal

charge-transfer processes from donor segments to acceptor segments. The HOMO and LUMO energy levels of **PCPDTBFQ** and **PDTSBFQ** trimers were calculated to be -4.39/-2.45, -4.44/-2.45 eV, respectively. The calculated band gaps were then determined to be 1.94, and 1.99 eV. From the calculation results, the bridging atom effect on the band gaps and energy levels is similar to those results obtained from CV and UV/vis evaluations. That is the introduction of Si atom will efficiently deepen the HOMO energy level and slightly increase the band gap.

Crystallinity and hole mobility

The crystallinity and molecular ordering property of the copolymer films were investigated by XRD analysis. Fig. 5a shows the XRD patterns of the corresponding polymer films casted from solutions in chlorobenzene (CB). As shown in Fig. 5a, the first peaks that are around 3.55 ° and 3.80 ° for **PCPDTBFQ** and **PDTSBFQ**, respectively, which are assignable to (100) diffraction of a lamellar structure. The *d*-spacing distance can be calculated to be about 24.9 Å and 23.2 Å. The shorter *d*-spacing distance and stronger diffraction peak were found from **PDTSBFQ** film, indicating a more ordered and tight packing in its solid state, which may result from the more linear molecular chains observed from the theoretical calculations. The broad (010) diffraction peaks give the information of π -stacking properties. **PCPDTBFQ** and **PDTSBFQ** films peak at about 20.5 ° and 22.0 °, featuring the π -stacking distances of 4.3 Å and 4.0 Å, respectively. It is clear that replacing the bridging C atom with a Si atom makes DTS-containing polymers favor a more planar geometry and a high degree of crystallinity.^{18c,18d} **PDTSBFQ** also shows a slight (200)

diffraction around 7.5° , which manifests again its excellent crystallinity as well.

The hole mobility of the active layer has a positive effect on the J_{sc} and fill factor (FF) of the resulting PSCs. Higher hole mobility is favorable in photovoltaic application because it can enable better carrier transport without large photocurrent loss caused by recombination of opposite charges.³⁵ To evaluation of the vertical charge carrier mobility, we fabricated hole-only devices to determine the space charge limited current (SCLC). This type of device was fabricated with a structure of indium tin oxide (ITO)/poly(3,4-ethylenedioxythiophene) (PEDOT):polystyrene sulfonate (PSS)/polymer/MoO₃/Au. The hole mobility can be calculated using the Mott-Gurney equation.³⁵ Fig. 5b shows the voltage (V)-current density (J) curves of the hole-only devices of the copolymer blends. The hole mobilities of **PCPDTBFQ** and **PDTSBFQ** were calculated to be $4.1 \times 10^{-6} \text{ cm}^2 \text{ V}^{-1} \text{ s}^{-1}$ and $1.5 \times 10^{-5} \text{ cm}^2 \text{ V}^{-1} \text{ s}^{-1}$, respectively. The **PDTSBFQ** film exhibits higher mobility than that of **PCPDTBFQ** film, which is attributed to the better crystallinity and molecular packing property, as described by the XRD analysis. The larger mobility of **PDTSBFQ** film is also highly desirable with respect to increasing the J_{sc} in its PSC devices.

Photovoltaic properties

To investigate the photovoltaic properties of **PCPDTBFQ** and **PDTSBFQ**, PSCs were first fabricated and evaluated with a device configuration of ITO/PEDOT:PSS/copolymer:PC₇₁BM/Ca/Al. The device performance was generally influenced by some processing parameters, such as the type of solvent, blend ratio of the copolymer and PC₇₁BM, annealing temperature, and the usage of processing

additives. The optimal weight ratio of copolymer to PC₇₁BM was found to be 1:1 (w/w). 3 vol % of 1,8-Diiodooctane (DIO) was added to blend solution to optimize the morphology of the active layer. In this work, the thermal annealing process had no effect on improving the device performance. The active layers were finally spin-coated from the polymers solutions with PC₇₁BM in CB, while the PFN interlayer was spin-coated from its methanol solution. All PSCs were tested under a simulated illumination (AM 1.5G, 100 mWcm⁻²). The current density-voltage (J-V) curves are plotted in Fig. 6a, and the data of photovoltaic parameters are listed in Table 3.

As shown in Fig. 6a, the **PDTSBFQ** device with a Ca interlayer exhibited a V_{oc} of 0.75 V, which is 0.4 V higher than that of **PCPDTBFQ** device. The elevated V_{oc} value is related to the lower-lying HOMO level of this polymer, measured from the CV experiments. The J_{sc} values of **PCPDTBFQ** and **PDTSBFQ** devices were 7.37 and 10.40 mA cm⁻², respectively. Generally, the J_{sc} is often affected by many factors, including the absorption property of the active layer and the charge carrier mobility. The higher J_{sc} agreed well with the higher hole mobility of **PDTSBFQ** determined from SCLC measurements (4.1×10^{-6} cm² V⁻¹ s⁻¹ for **PCPDTBFQ** and 1.5×10^{-5} cm² V⁻¹ s⁻¹ for **PDTSBFQ**). The improved J_{sc} was also confirmed by the external quantum efficiency (EQE) evaluation. As shown in Fig. 6b, the photocurrent response of both devices covered the range of 300-800 nm. But **PDTSBFQ** showed a little broader but much higher curve shape. The maximum EQE plateau of **PDTSBFQ** reached 53%, which was higher than that of **PCPDTBFQ** (38%), resulting in more efficient light

harvesting and higher J_{sc} values as well. Furthermore, the J_{sc} values calculated by integrating the EQE curves with an AM 1.5G reference spectrum are within 3% error compared to the corresponding J_{sc} values obtained from the J-V curves. Obviously, the better optical response and higher carrier mobility guarantee **PDTSBFQ** device to achieve a larger J_{sc} value. The elevation of sixteen percentage points in FF had also been obtained from **PDTSBFQ** device (FF=0.57) compared with **PCPDTBFQ** device (FF=0.41). The result can be attributed to the formation of the optimal blend film morphology. The surface morphology of polymer:PC₇₁BM film was checked by using atomic force microscopy (AFM). The AFM height (left) and phase (right) images are shown in Fig. 7. The blend films of **PCPDTBFQ** and **PDTSBFQ** showed different morphological properties. The average surface roughnesses (R_a) measured from the topographic images were 1.15 and 2.02 nm for **PCPDTBFQ** and **PDTSBFQ** blend films, respectively, casting from CB solution with ratios of 1:1 (by adding 3% DIO). The R_a of **PDTSBFQ** blend film is about 1.8 folds of that of **PCPDTBFQ** film. However, **PCPDTBFQ** film possesses a poorer nanoscale phase separation (see the phase images). The aggregation size of **PCPDTBFQ** film reached more than one hundred nanometer scale, which is the much bigger than that of **PDTSBFQ** film. This is due to the bad compatibility of **PCPDTBFQ** and PC₇₁BM. On the contrary, the aggregation size in the **PDTSBFQ** blend film was in an ideal region of 10-20 nm, which would not cause strong geminate recombination, giving rise to a higher FF and a more efficient EQE of **PDTSBFQ** devices. This result also indicated that the bridging atom effect had a distinct influence on the compatibility and aggregation of

the blend counterparts. As a result, a 4.43% PCE of **PDTSBFQ** device was achieved, which was about 2 times of that of **PDTSBFQ** device (2.16%) under the same conditions.

Because PFN interfacial layer could largely elevate the photovoltaic performance of a group of N-heterocycle-containing polymer donors.³⁶ In order to study the effect of different top electrode, we fabricated another type of PSC devices with a structure of ITO/PEDOT:PSS/copolymer:PC₇₁BM/PFN/Al. After using a PFN/Al instead of the Ca/Al top cathode, the PSCs based on both copolymers exhibited largely enhanced performance. **PCPDTBFQ** and **PDTSBFQ** devices showed PCEs of 3.23% and 5.92%, respectively, which had a great increase of 50% and 34% in comparison with those with a Ca/Al cathode. In comparison of both type of devices, the V_{oc} just elevated a little. So the increased PCEs were mainly attributed to the improvements of J_{sc} and FF. For **PCPDTBFQ** and **PDTSBFQ** devices, the J_{sc} values were increased from 7.37 to 8.55 mA cm⁻², and from 10.39 to 12.25 mA cm⁻². But the FF values were largely increased from 0.41 to 0.57, and 0.52 to 0.63 for **PCPDTBFQ** and **PDTSBFQ** devices, respectively. This elevation of J_{sc} and FF were also checked by EQE curves, as shown in Fig. 6b. The maximum EQE values were raised from 38% to 43%, and 53% to 63%, for **PCPDTBFQ** and **PDTSBFQ** devices, respectively. Clearly, **PCPDTBFQ** and **PDTSBFQ** contain enough N atoms, supplying the strong N-N interactions at the interface between the polymers and PFN layer.³⁶ Such polar effect can establish good interface contact with the Al cathode, enhancing the electron extraction from the acceptor phase to the metal cathode and decreasing the hole-electron recombination in

the active layer. As a result, enhanced J_{sc} and FF values were obtained to achieve the high PCE near 6% in PSCs from DTS-FQ_x conjugated copolymers.

Conclusion

Two novel fluorinated quinoxaline-based alternating copolymers, **PCPDTBFQ** and **PDTSBFQ**, have been successfully synthesized and characterized, incorporated with C-bridged cyclopentadithiophene (CPDT) or Si-bridged dithienosilole (DTS) blocks. The bridging atom effect showed a great influence on the absorption property, energy level, carrier mobility and photovoltaic performance of the resulting copolymers. When using DTS block instead of CPDT, **PDTSBFQ** showed a little blue-shift as well as a little larger band gap than those of **PCPDTBFQ**. However, **PDTSBFQ** showed unique aggregation even in solution state. The electrochemical results indicated that **PDTSBFQ** had a lower-lying HOMO level, implying that a high V_{oc} could be obtained in its PSCs. From XRD analysis, **PDTSBFQ** also exhibited the better crystallinity and molecular ordering property than **PCPDTBFQ**, which induced a higher hole mobility ($1.5 \times 10^{-5} \text{ cm}^2 \text{ V}^{-1} \text{ s}^{-1}$ for **PDTSBFQ** and $4.1 \times 10^{-6} \text{ cm}^2 \text{ V}^{-1} \text{ s}^{-1}$ for **PCPDTBFQ**) measured by SCLC method. BHJ solar cell devices were finally fabricated to investigate the photovoltaic properties of these two copolymers. Different interfacial layer (IFL) had also been tried to optimize the performance of the fabricated PSCs. When using a Ca/Al top electrode, **PDTSBFQ** device showed a PCE of 4.43% while **PCPDTBFQ** device just had a lower PCE of 2.16%. This enhancement would thank for the elevations of V_{oc} , J_{sc} and FF values. After replacing the Ca/Al with a PFN/Al cathode, the performance of both **PCPDTBFQ** and

PDTSBFQ devices were enhanced largely. Then, **PDTSBFQ** device achieved the highest PCE of 5.92%. All these results confirmed our design strategy and afforded a simple but efficient approach to obtain the high performance dithiophene-quinoxaline polymer donors by bridging atom effect and fluorinated substitution.

Experimental section

Measurements and characterization

The nuclear magnetic resonance (NMR) spectra were collected on a Bruker ARX 400 NMR spectrometer with *d*-chloroform as the solvent and tetramethylsilane (TMS) as the internal standard. Elemental analysis was performed using a Carlo Erba 116 elemental analyzer. Molecular weights of the copolymers were determined using Waters 1515 GPC analysis with chloroform as eluent at 35 °C and 80 °C, and polystyrene as standard. Thermogravimetric analysis (TGA) was conducted on a TA Instrument Model SDT Q600 simultaneous TGA/DSC analyzer at a heating rate of 10 °C min⁻¹ under a N₂ flow rate of 90 mL min⁻¹. UV-vis spectra were obtained on a Carry 300 spectrophotometer. Cyclic voltammetry (CV) measurements were carried out at room temperature on a CHI660 potentiostat/galvanostat electrochemical workstation at a scan rate of 50 mV s⁻¹, with a platinum wire counter electrode and an Ag/AgCl reference electrode in an anhydrous nitrogen-saturated acetonitrile solution (0.1 mol⁻¹) of tetrabutylammonium perchlorate (Bu₄NClO₄). The redox couple of ferrocene/ferrocenium ion (Fc/Fc⁺) was used as an external standard. The copolymers were coated on the platinum plate working electrodes from dilute chloroform solutions. XRD patterns of the polymers were recorded on a Philips X-ray

diffractometer operated in reflection geometry at 30 mA, 40 kV with $\text{Cu}_{K\alpha}$ radiation. The AFM measurements were performed on a Veeco Nanoscope V microscope in tapping mode.

PSC device fabrication and characterization

PSCs were fabricated with ITO glass ($15 \Omega \text{ cm}^{-2}$) as the anode, Ca/Al or PFN/Al as the cathode, and the active layer of the copolymer and PC_{71}BM as the photosensitive layer. After spin-coating a 35 nm layer of PEDOT:PSS (Baytron P VP Al 4083) onto the pre-cleaned ITO substrate, the photosensitive layer was subsequently prepared by spin-coating the solution (by adding 3% DIO) of the copolymer and PC_{71}BM (w/w) in CB on the ITO/PEDOT:PSS electrode. The device area was 0.09 cm^2 . I-V characterization of the devices was carried out on a computer-controlled Keithley 236 Source Measurement system. The EQE values were measured at a chopping frequency of 280 Hz with a lock-in amplifier (Stanford, SR830 DSP) during illumination with monochromatic light from a xenon lamp. A solar simulator was used as the light source, and the light intensity was monitored by using a standard Si solar cell. The thickness of the films was measured by using a Dektak 6M surface profilometer. All fabrication and characterization processes, except for the EQE measurements, were conducted in a glove box.

Materials

All chemicals were purchased as reagent grade from Aladdin, Adamas, Aldrich, Alfa Aesar, and Acros Chemical Co., and used without further purification. All solvents were freshly distilled immediately prior to use. Monomer **BFQ** and the other two

organic tin monomers were synthesized according to the procedures of the published literatures.^{17,21}

PCPDTBFQ

5,5'-bis(tributylstannyl)-4,4-dioctyl-cyclopenta[2,1-b:3,4-b']dithiophene (0.2942 g, 0.3000 mmol), monomer **BFQ** (0.2628 g, 0.3000 mmol), and degassed toluene (12 mL) were added to a two-necked flask. After being degassed with argon several times, Pd₂(dba)₃ (5.5 mg, 2 mol%) and P(*o*-tol)₃ (7.3 mg, 8%) were added and the solution was degassed with argon several times again. The reaction solution was subsequently heated to 110 °C for 24 h. Tributylstannylthiophene (23.7 mL) was added to the reaction and then after 2 h, 2-bromothiophene (7.5 mL) was added. The mixture was stirred overnight to complete the end-capping reaction. The reactant mixture was slowly dropped into methanol (400 mL) to allow precipitation of the crude polymer. The precipitate was then filtered, and washed with methanol and hexane in a Soxhlet apparatus to remove oligomers and catalyst residue. Finally, the copolymer was extracted with chloroform. The solution was condensed by evaporation and precipitated into methanol again. The purified **PCPDTBFQ** was then collected as a dark-purple solid (0.28 g, 83 %). ¹H NMR (400MHz, CDCl₃, δ/ppm): 8.2-6.7 (m, 15H, ArH), 4.1-3.7 (m, 4H, -O-CH₂-), 2.1-1.0 (m, 52H, -CH₂-), 1.0-0.7 (m, 12H, -CH₃). Anal. calcd for (%) for (C₆₉H₈₃O₂N₂S₄F)_n: C 74.02, H 7.47, N 2.50; found: C 73.83, H 7.58, N, 2.27.

PDTSBFQ

Polymer **PDTSBFQ** was obtained as a dark-purple solid in a yield of 85% from the

reaction of 4,4'-bis(n-octyl)-2,2'-bis(tributylstannyl)-dithieno[3,2-b:2',3'-d]silole with monomer **BFQ**, similar to the procedure described for **PCPDTBFQ**. ^1H NMR (400MHz, CDCl_3 , δ/ppm): 8.5-6.4 (m, 15H, ArH), 4.1-3.7 (m, 4H, $-\text{OCH}_2-$, 4H, $-\text{CH}_2-$), 2.0-1.0 (m, 48H, $-\text{CH}_2-$), 1.0-0.7 (m, 12H, $-\text{CH}_3$). Anal. calcd for (%) for $(\text{C}_{68}\text{H}_{83}\text{O}_2\text{N}_2\text{S}_4\text{FSi})_n$: C 71.91, H 7.37, N 2.47; found: C 72.19, H 7.15, N: 2.31.

Acknowledgements

This work was supported by the NSFC (21272164, 21432005), the 863 Project (No: 2013AA031901), the Youth Science and Technology Foundation of Sichuan Province (2013JQ0032), the Foundation of State Key Laboratory of Polymer Materials Engineering (sklpme2014-3-05), and the Fundamental Research Funds for the Central Universities (2012SCU04B01, YJ2011025). We also appreciate the comprehensive training platform of specialized laboratory, college of chemistry, sichuan University, for the NMR, elemental analysis, DSC, TGA measurements.

References

- 1 (a) S. Günes, H. Neugebauer and N. S. Sariciftci, *Chem. Rev.*, 2007, **107**, 1324-1338; (b) Y. J. Cheng, S. H. Yang and C. S. Hsu, *Chem. Rev.*, 2009, **109**, 5868-5923; (c) G. Li, R. Zhu and Y. Yang, *Nat. Photonics*, 2012, **6**, 153-161; (d) J. You, L. Dou, K. Yoshimura, T. Kato, K. Ohya, T. Moriarty, K. Emery, C. C. Chen, J. Gao, G. Li, Y. Yang, *Nat. Commun.*, 2013, **4**, 1446-1455.
- 2 (a) J. W. Chen and Y. Cao, *Acc. Chem. Res.*, 2009, **42**, 1709-1718; (b) L. Dou, J. You, J. Yang, C.-C. Chen, Y. He, S. Murase, T. Moriarty, K. Emery, G. Li and Y. Yang, *Nat. Photonics*, 2012, **6**, 180-185.

- 3 (a) Z. He, C. Zhong, S. Su, M. Xu, H. Wu and Y. Cao, *Nat. Photonics*, 2012, **6**, 591-595; (b) S. H. Liao, H. J. Jhuo, Y. S. Cheng and S. A. Chen, *Adv. Mater.*, 2013, **25**, 4766-4771; (c) C. C. Chen, W. H. Chang, K. Yoshimura, K. Ohya, J. You, J. Gao, Z. Hong and Y. Yang, *Adv. Mater.*, 2014, **26**, 5670-5677; (d) W. Zhang, Y. Wu, Q. Bao, F. Gao and J. Fang, *Adv. Energy Mater.*, 2014, DOI: 10.1002/aenm.201400359.
- 4 (a) H. Usta, G. Lu, A. Facchetti and T. J. Marks, *J. Am. Chem. Soc.*, 2006, **128**, 9034-9035; (b) M. Wang, X. Hu, P. Liu, W. Li, X. Gong, F. Huang and Y. Cao, *J. Am. Chem. Soc.*, 2011, **133**, 9638-9641; (c) Q. Peng, Q. Huang, X. Hou, P. Chang, J. Xu, and S. Deng, *Chem. Commun.*, 2012, **48**, 11452-11454; (d) S. Li, Z. Yuan, P. Deng, B. Sun and Q. Zhang, *Polym. Chem.*, 2014, **5**, 2561-2566.
- 5 (a) Z. G. Zhang and J. Wang, *J. Mater. Chem.*, 2012, **22**, 4178-4187; (b) L. A. Perez, P. Zalar, L. Ying, K. Schmidt, M. F. Toney, T. Q. Nguyen, G. C. Bazan and E. J. Kramer, *Macromolecules*, 2014, **47**, 1403-1410.
- 6 (a) T. Qin, W. Zajaczkowski, W. Pisula, M. Baumgarten, M. Chen, M. Gao, G. Wilson, C. D. Easton, K. Müllen and S. E. Watkins, *J. Am. Chem. Soc.*, 2014, **136**, 6049-6055; (b) M. Wang, H. Wang, T. Yokoyama, X. Liu, Y. Huang, Y. Zhang, T. Q. Nguyen, S. Aramaki and G. C. Bazan, *J. Am. Chem. Soc.*, 2014, **136**, 12576-12579.
- 7 Q. Peng, X. Liu, D. Su, G. Fu, J. Xu and L. Dai, *Adv. Mater.*, 2011, **23**, 4554-4558.
- 8 (a) J. Y. Kim, K. Lee, N. E. Coates, D. Moses, T. Q. Nguyen, M. Dante, A. J. Heeger, *Science*, 2007, **317**, 222-225; (b) W. Li, A. Furlan, K. H. Hendriks, M. M. Wienk and R. A. J. Janssen, *J. Am. Chem. Soc.*, 2013, **135**, 5529-5532; (c) K. Li, Z.

- Li, K. Feng, X. Xu, L. Wang and Q. Peng, *J. Am. Chem. Soc.*, 2013, **135**, 13549-13557; (d) L. Dou, W. H. Chang, J. Gao, C. C. Chen, J. You and Y. Yang, *Adv. Mater.*, 2013, **25**, 825-831; (e) A. R. B. M. Yusoff, S. J. Lee, H. P. Kim, F. K. Shneider, W. J. D. Silva and J. Jang, *Adv. Funct. Mater.*, 2014, **24**, 2240-2247.
- 9 E. Zhou, S. Yamakawa, K. Tajima, C. Yang and K. Hashimoto, *Chem. Mater.*, 2009, **21**, 4055-4061.
- 10 (a) H. Zhou, L. Yang, S. Stoneking, W. You, *ACS Appl. Mater. Interfaces*, 2010, **2**, 1377-1383; (b) H. Zhou, L. Yang, S. C. Price, K. J. Knight and W. You, *Angew. Chem. Int. Ed.*, 2010, **49**, 7992-7995.
- 11 (a) C. V. Hoven, X. D. Dang, R. C. Coffin, J. Peet, T. Q. Nguyen and G. C. Bazan, *Adv. Mater.*, 2010, **22**, E63-E66; (b) T. Y. Chu, J. Lu, S. Beaupré, Y. Zhang, J. R. Pouliot, S. Wakim, J. Zhou, M. Leclerc, Z. Li, J. Ding and Y. Tao, *J. Am. Chem. Soc.*, 2011, **133**, 4250-4253; (c) H. Zhou, L. Yang, A. C. Stuart, S. C. Price, S. Liu and W. You, *Angew. Chem. Int. Ed.*, 2011, **50**, 2995-2998; (d) S. Albrecht, S. Janietz, W. Schindler, J. Frisch, J. Kurpiers, J. Kniepert, S. Inal, P. Pingel, K. Fostiropoulos, N. Koch and D. Neher, *J. Am. Chem. Soc.*, 2012, **134**, 14932-14944; (e) N. Wang, Z. Chen, W. Wei and Z. Jiang, *J. Am. Chem. Soc.*, 2013, **135**, 17060-17068; (f) J. Warnan, C. Cabanetos, A. E. Labban, M. R. Hansen, C. Tassone, M. F. Toney and P. M. Beaujuge, *Adv. Mater.*, 2014, **26**, 4357-4362.
- 12 (a) S. Liu, K. Zhang, J. Lu, J. Zhang, H. L. Yip, F. Huang and Y. Cao, *J. Am. Chem. Soc.*, 2013, **135**, 15326-15329; (b) X. Guo, M. Zhang, W. Ma, L. Ye, S. Zhang, S. Liu, H. Ade, F. Huang and J. Hou, *Adv. Mater.*, 2014, **26**, 4043-4049.

- 13 (a) E. Wang, L. Hou, Z. Wang, S. Hellström, F. Zhang, O. Inganäs and M. R. Andersson, *Adv. Mater.*, 2010, **22**, 5240-5244; (b) Y. Zhang, J. Zou, H. L. Yip, K. S. Chen, D. F. Zeigler, Y. Sun and A. K. Y. Jen, *Chem. Mater.*, 2011, **23**, 2289-2291; (c) Y. Kim, H. R. Yeom, J. Y. Kim and C. Yang, *Energy Environ. Sci.*, 2013, **6**, 1909-1916.
- 14 (a) H. C. Chen, Y. H. Chen, C. C. Liu, Y. C. Chien, S. W. Chou and P. T. Chou, *Chem. Mater.*, 2012, **24**, 4766-4772; (b) Y. Lu, Z. Xiao, Y. Yuan, H. Wu, Z. An, Y. Hou, C. Gao and J. Huang, *J. Mater. Chem. C*, 2013, **1**, 630-637; (c) W. Zhuang, H. Zhen, R. Kroon, Z. Tang, S. Hellström, L. Hou, E. Wang, D. Gedefaw, O. Inganäs, F. Zhang and M. R. Andersson, *J. Mater. Chem. A*, 2013, **1**, 13422-13425.
- 15 A. Iyer, J. Bjorgaard, T. Anderson and M. E. Köse, *Macromolecules*, 2012, **45**, 6380-6389.
- 16 A. C. Stuart, J. R. Tumbleston, H. Zhou, W. Li, S. Liu, H. Ade and Wei You, *J. Am. Chem. Soc.*, 2013, **135**, 1806-1815.
- 17 X. Xu, Y. Wu, J. Fang, Z. Li, Z. Wang, Y. Li and Q. Peng, *Chem. Eur. J.*, 2014, **20**, 13259-13271.
- 18 (a) J. Peet, J. Y. Kim, N. E. Coates, W. L. Ma, D. Moses, A. J. Heeger and G. C. Bazan, *Nat. Mater.*, 2007, **6**, 497-500; (b) R. C. Coffin, J. Peet, J. Rogers and G. C. Bazan, *Nat. Chemistry*, 2009, **1**, 657-661; (c) M. C. Scharber, M. Koppe, J. Gao, F. Cordella, M. A. Loi, P. Denk, M. Morana, H. J. Egelhaaf, K. Forberich, G. Dennler, R. Gaudiana, D. Waller, Z. Zhu, X. Shi and C. J. Brabec, *Adv. Mater.*, 2010, **22**, 367-370; (d) H. Y. Chen, J. Hou, A. E. Hayden, H. Yang, K. N. Houk and

- Y. Yang, *Adv. Mater.*, 2010, **22**, 371-375.
- 19 (a) L. Huo, J. Hou, H. Y. Chen, S. Zhang, Y. Jiang, T. L. Chen and Y. Yang, *Macromolecules*, 2009, **42**, 6564-6571; (b) J. Hou, T. L. Chen, S. Zhang, H.-Y. Chen and Y. Yang, *J. Phys. Chem. C*, 2009, **113**, 1601-1605.
- 20 (a) A. J. Moulé, A. Tsami, T. W. Bünnagel, M. Forster, N. M. Kronenberg, Markus Scharber, M. Koppe, M. Morana, C. J. Brabec, K. Meerholz and U. Scherf, *Chem. Mater.*, 2008, **20**, 4045-4050; (b) C. H. Chen, C. H. Hsieh, M. Dubosc, Y. J. Cheng and C. S. Hsu, *Macromolecules* 2010, **43**, 697-708; (c) M. C. Yuan, M. Y. Chiu, C. M. Chiang and K. H. Wei, *Macromolecules*, 2010, **43**, 6270-6277; (d) Y. J. Cheng, Y. J. Ho, C. Hsiang Chen, W. S. Kao, C. E. Wu, S. L. Hsu and C. S. Hsu, *Macromolecules*, 2012, **45**, 2690-2698.
- 21 (a) J. Z. Brzezinski and J. R. Reynolds, *Synthesis*, 2002, 1053-1056; (b) P. Coppo, D. C. Cupertino, S. G. Yeates and M. L. Turner. *Macromolecules*, 2003, **36**, 2705-2711; (c) X. Guo, F. S. Kim, M. J. Seger, S. A. Jenekhe and M. D. Watson. *Chem. Mater.*, 2012, **24**, 1434-1442; (d) G. Lu, H. Usta, C. Risko, L. Wang, A. Facchetti, M. A. Ratner and T. J. Marks. *J. Am. Chem. Soc.*, 2008, **130**, 7670-7685; (e) P. M. Beaujuge, H. N. Tsao, M. R. Hansen, C. M. Amb, C. Risko, J. Subbiah, K. R. Choudhury, A. Mavrinskiy, W. Pisula, J. L. Brédas, F. So, K. Müllen and J. R. Reynolds. *J. Am. Chem. Soc.*, 2012, **134**, 8944-8957.
- 22 Y. Wang, F. Yang, Y. Liu, R. Peng, S. Chen and Z. Ge, *Macromolecules*, 2013, **46**, 1368-1375.
- 23 J. M. Jiang, P. A. Yang, C. M. Yu, H. K. Lin, K. C. Huang, K. H. Wei, *J. Polym. Sci.*

- Part A: Polym. Chem.*, 2012, **50**, 3960-3969.
- 24 Z. B. Henson, G. C. Welch, T. Poll and G. C. Bazan, *J. Am. Chem. Soc.*, 2012, **134**, 3766-3779.
- 25 G. C. Welch, L. A. Perez, C. V. Hoven, Y. Zhang, X. D. Dang, A. Sharenko, M. F. Toney, E. J. Kramer, T. Q. Nguyen and G. C. Bazan, *J. Mater. Chem.*, 2011, **21**, 12700-12709.
- 26 Y. F. Li, *Acc. Chem. Res.*, 2012, **45**, 723-733.
- 27 (a) Y. F. Li, Y. Cao, J. Gao, D. L. Wang, G. Yu and A. J. Heeger, *Synth. Met.*, 1999, **99**, 243-248; (b) Q. Peng, Z. Y. Lu, Y. Huang, M. G. Xie, S. H. Han, J. B. Peng and Y. Cao, *Macromolecules*, 2004, **37**, 260-266; (c) Q. Peng, J. B. Peng, E. T. Kang, K. G. Neoh and Y. Cao, *Macromolecules*, 2005, **38**, 7292-7298.
- 28 X. G. Guo, F. S. Kim, M. J. Seger, S. A. Jenekhe, M. D. Watson, *Chem. Mater.*, 2012, **24**, 1434-1442.
- 29 (a) N. S. Sariciftci, *Primary Photoexcitations in Conjugated Polymers: Molecular Excitations vs Semiconductor Band Model*; World Scientific: Singapore, 1997; (b) P. T. Wu, F. S. Kim, R. D. Champion and S. A. Jenekhe, *Macromolecules*, 2008, **41**, 7021-7028.
- 30 (a) C. J. Brabec, A. Cravino, D. Meissner, N. S. Sariciftci, T. Fromherz, M. T. Rispens, L. Sanchez and J. C. Hummelen, *Adv. Funct. Mater.*, 2001, **11**, 374-380; (b) M. C. Scharber, D. Mühlbacher, M. Koppe, P. Denk, C. Waldauf, A. J. Heeger and C. J. Brabec, *Adv. Mater.*, 2006, **18**, 789-794.
- 31 (a) J. S. Wu, Y. J. Cheng, T. Y. Lin, C. Y. Chang, P. I. Shih, C. S. Hsu, *Adv. Funct.*

- Mater.*, 2012, **22**, 1711-1722; (b) Y. C. Pao, Y. L. Chen, Y. T. Chen, S. W. Cheng, Y. Y. Lai, W. C. Huang, Y. J. Cheng, *Org. Lett.*, 2014, **16**, 5724-5727.
- 32 C. J. Brabec, C. Winder, N. S. Sariciftci, J. C. Hummelen, A. Dhanabalan, P. A. van Hal and R. A. J. Janssen, *Adv. Funct. Mater.*, 2002, **12**, 709-712.
- 33 (a) H. C. Chen, Y. H. Chen, C. H. Liu, Y. H. Hsu, Y. C. Chien, W. T. Chuang, C. Y. Cheng, C. L. Liu, S. W. Chou, S. H. Tung and P. T. Chou, *Polym. Chem.*, 2013, **4**, 3411-3418; (b) P. Y. Yang, M. J. Yuan, D. F. Zeigler, S. E. Watkins, J. A. Leeb and C. K. Luscombe, *J. Mater. Chem. C*, 2014, **2**, 3278-3284.
- 34 G. L. Gibson, T. M. McCormick and D. S. Seferos, *J. Phys. Chem. C*, 2013, **117**, 16606-16615.
- 35 (a) X. Guo, N. Zhou, S. J. Lou, J. W. Hennek, O. R. Ponce, M. R. Butler, P. L. Boudreault, J. Strzalka, P. O. Morin, M. Leclerc, N. J. T. Lopez, M. A. Ratner, L. X. Chen, R. P. Chang, A. Facchetti and T. J. Marks, *J. Am. Chem. Soc.*, 2012, **134**, 18427-18439; (b) Q. Peng, S. L. Lim, I. H. Wong, J. Xu, Z. K. Chen, *Chem. Eur. J.*, 2012, **18**, 12140-12151; (c) Z. G. Wang, J. Zhao, Y. Li, Q. Peng, *Polym. Chem.*, 2014, **5**, 4984-4992; (d) Y. C. Yang, R. M. Wu, X. Wang, X. P. Xu, Z. J. Li, K. Li and Q. Peng, *Chem. Commun.*, 2014, **50**, 439-441.
- 36 Z. C. He, C. Zhang, X. F. Xu, L. J. Zhang, L. Huang, J. W. Chen, H. B. Wu, Y. Cao, *Adv. Mater.*, 2011, **23**, 3086-3089.

Legends for Schemes, Figures and Tables

Scheme 1 Design strategy and molecular structures of the copolymers.

Scheme 2 Synthetic routes of the copolymers.

Fig. 1 Thermogravimetric analysis (TGA) and differential scanning calorimetry (DSC) curves of the copolymers.

Fig. 2 Normalized UV-vis absorption spectra of the copolymers (a) by low vibration energy peaks in chloroform solutions (10^{-5} M) and thin solid films; (b) by low vibration energy peaks in chloroform solutions (10^{-6} M); (c) and (d) by high vibration energy peaks in diluted and heated chloroform solutions.

Fig. 3 (a) Cyclic voltammograms (CV) of the copolymers at a scan rate of 50 mV s^{-1} . (b) the electronic energy level diagram of the copolymers and PC₇₁BM.

Fig. 4 Molecular structures and optimized molecular orbital surfaces of the LUMO+1, LUMO, HOMO and HOMO-1 for the model trimers, obtained by Gaussian 09 at the B3LYP/6-31G(d) level.

Fig. 5 (a) X-ray diffraction patterns of the copolymer films on silicon wafers. (b) J-V characteristics of copolymer/PC₇₁BM-based hole-only devices measured at ambient temperature.

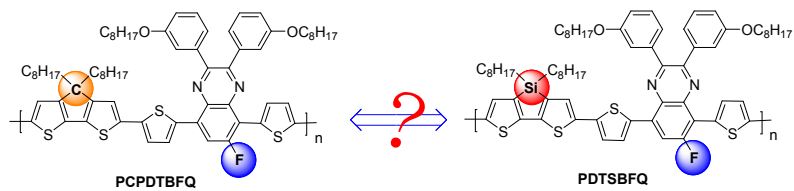
Fig. 6 (a) J-V curves of co-polymer:PC₇₁BM (1:1) based PSCs under AM 1.5G illumination, 100 mWcm^{-2} . (b) EQE curves of copolymer:PC₇₁BM (1:1) based PSCs.

Fig. 7 AFM topographic images of the film blends (polymer:PC₇₁BM=1:1, w/w). (a, b) PCPDTBFQ, (c, d) PDTSBFQ. Image size: $5 \times 5 \text{ }\mu\text{m}^2$.

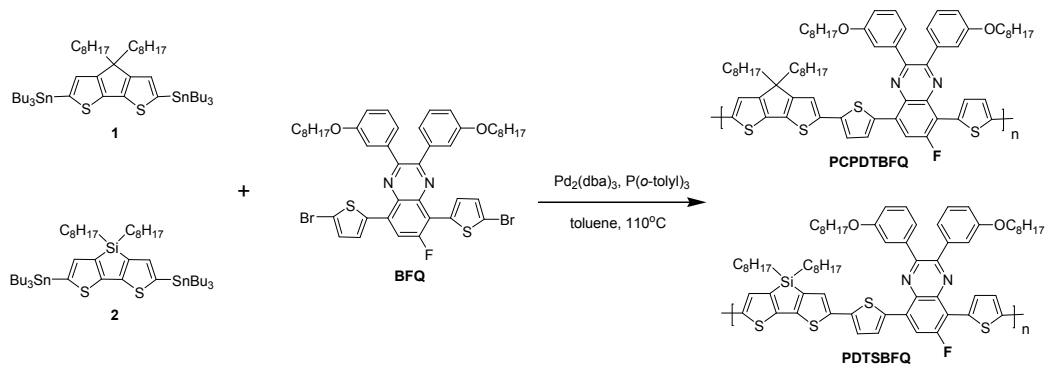
Table 1 Molecular weights and thermal data of the copolymers.

Table 2 Optical and electrochemical data of the copolymers.

Table 3 Performance of polymer solar cells tested under AM 1.5 simulated illumination.



Scheme 1. Design strategy and molecular structures of the copolymers.



Scheme 2. Synthetic routes of the copolymers.

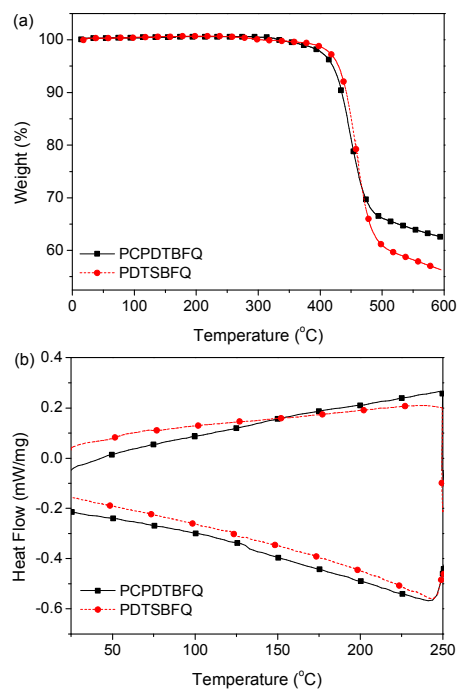


Fig. 1 Thermogravimetric analysis (TGA) and differential scanning calorimetry (DSC) curves of the copolymers.

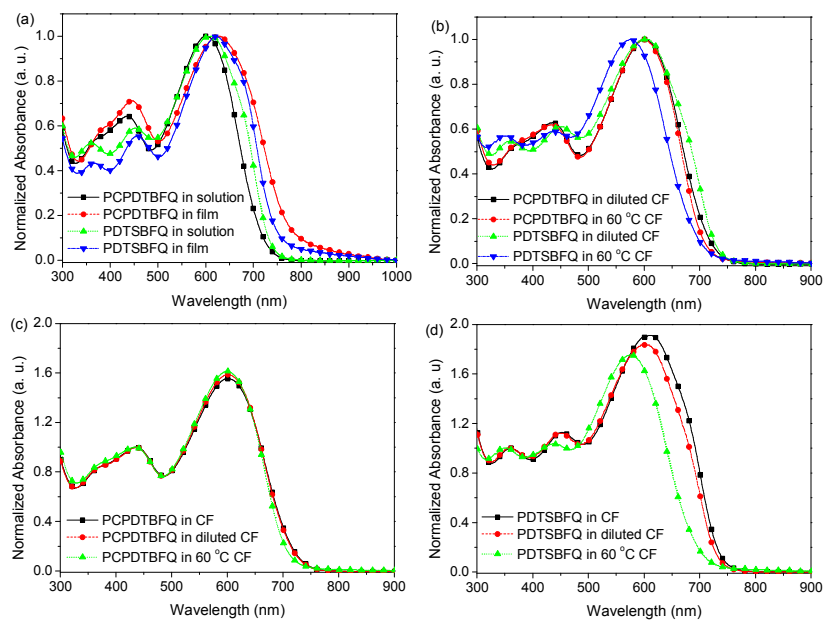


Fig. 2 Normalized UV-vis absorption spectra of the copolymers (a) by low vibration energy peaks in chloroform solutions (10^{-5} M) and thin solid films; (b) by low vibration energy peaks in chloroform solutions (10^{-6} M); (c) and (d) by high vibration energy peaks in diluted and heated chloroform solutions.

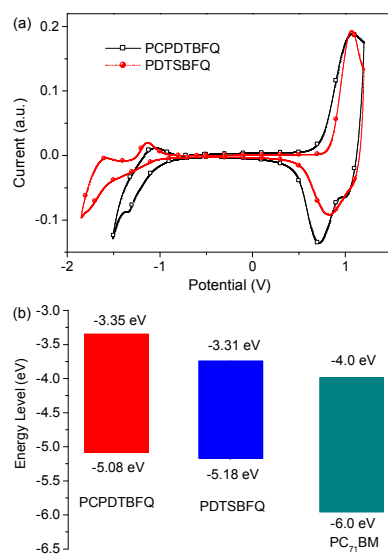


Fig. 3 (a) Cyclic voltammograms (CV) of the copolymers at a scan rate of 50 mV s^{-1} . (b) the electronic energy level diagram of the copolymers and PC₇₁BM.

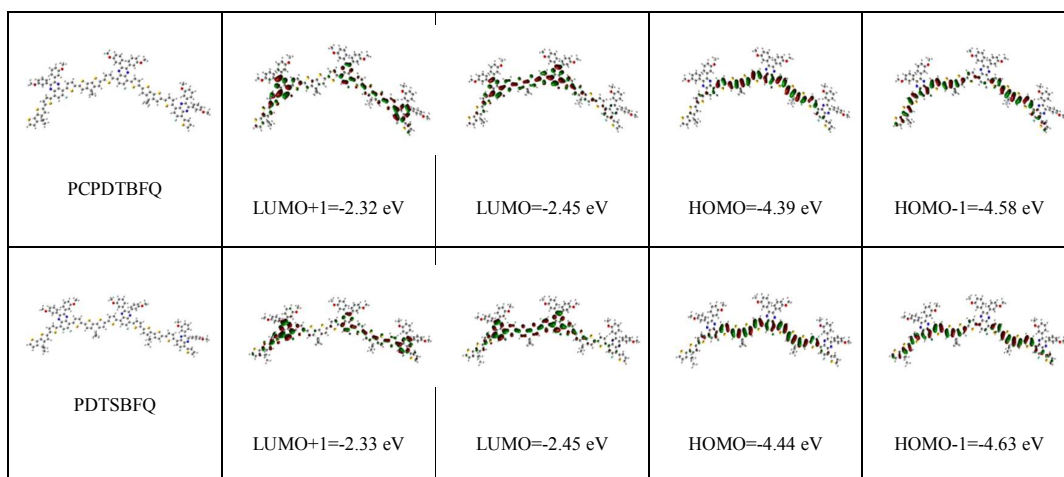


Fig. 4 Molecular structures and optimized molecular orbital surfaces of the LUMO+1, LUMO, HOMO and HOMO-1 for the model trimers, obtained by Gaussian 09 at the B3LYP/6-31G(d) level.

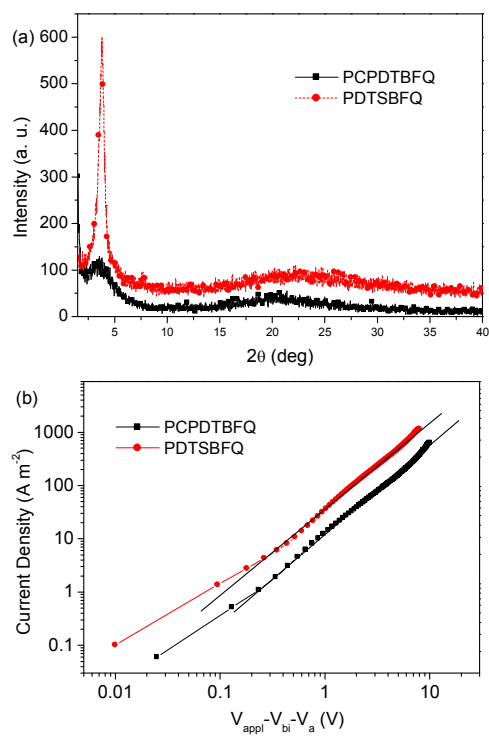


Fig. 5 (a) X-ray diffraction patterns of the copolymer films on silicon wafers.(b) J-V characteristics of copolymer-based hole-only devices measured at ambient temperature.

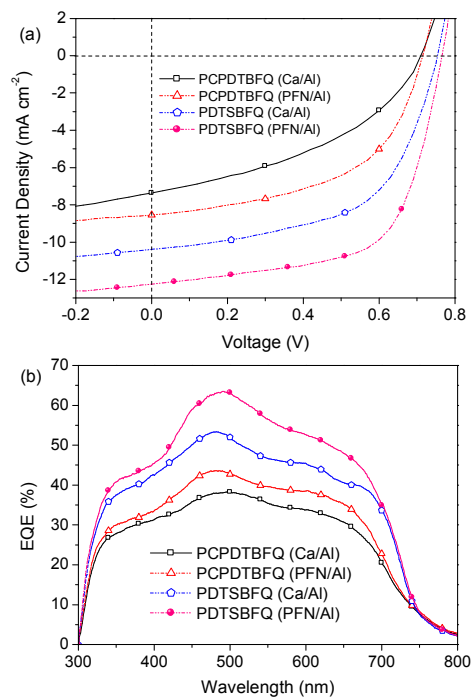


Fig. 6 (a) J-V curves of co-polymer:PC₇₁BM (1:1) based PSCs under AM 1.5G illumination, 100 mWcm⁻². (b) EQE curves of copolymer:PC₇₁BM (1:1) based PSCs.

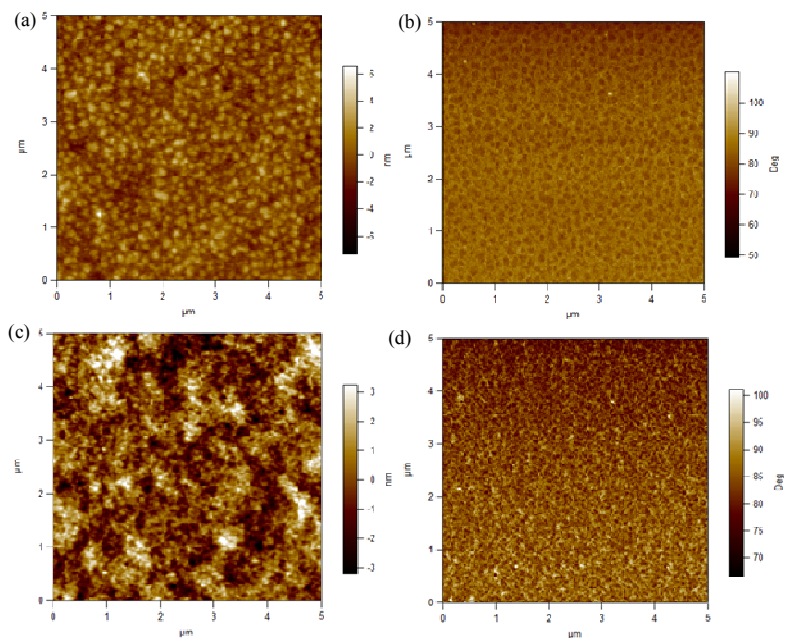


Fig. 7 AFM topographic images of the film blends (polymer:PC₇₁BM=1:1, w/w). (a, b)

PCPDTBFQ, (c, d) PDTSBFQ. Image size: 5×5 μm².

Table 1. Molecular weights and thermal data of the copolymers.

Copolymers	Yield (%)	M _w ^[a] (kDa)	M _n ^[a] (kDa)	PDI ^[a]	T _d ^[b] (°C)
PCPDTBFQ	83.4	36	16	2.2	421
PDTSBFQ	85.2	223	34	6.5	430

[a]Molecular weights and polydispersity indices were determined by GPC in THF using the polystyrene as a standard. [b]Onset decomposition temperatures were measured by TGA under N₂.

Table 2. Optical and electrochemical data of the copolymers.

Copolymers	Abs. (nm)	Abs. (nm)	$E_g^{[a]}$	HOMO	LUMO	$E_g^{[b]}$
	λ_{\max}^{Sol}	λ_{\max}^{film}	(eV)	(eV)	(eV)	(eV)
PCPDTBFQ	600,436	627,446	1.60	-5.08	-3.35	1.73
PDTSBFQ	612,453,360	623,456,365	1.63	-5.18	-3.31	1.87

[a]Optical band gap was estimated from the wavelength of the optical absorption edge of the copolymer film. [b]Electrochemical band gap was calculated from the LUMO and HOMO energy levels.

Table 3 Performance of polymer solar cells tested under AM 1.5 simulated illumination.

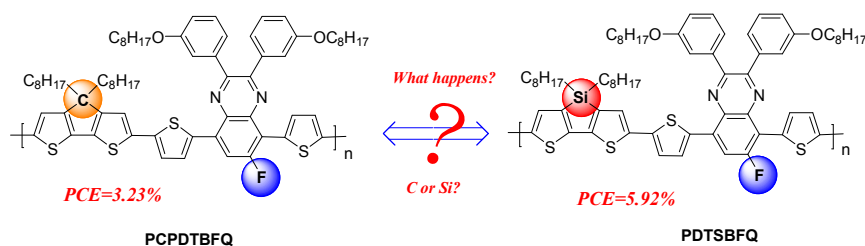
Copolymers	thickness (nm)	V _{oc} (V)	J _{sc} (mA cm ⁻²)	FF	PCE (%)
PCPDTBFQ ^a	105	0.71	7.37	0.41	2.16
PCPDTBFQ ^b	100	0.72	8.55	0.53	3.23
PDTSBFQ ^a	102	0.75	10.40	0.57	4.43
PDTSBFQ ^b	96	0.77	12.25	0.63	5.92

^aUsing a Ca/Al top electrode. ^bUsing a PFN/Al top electrode.

The table of contents entry

Enhanced Performance of Fluorinated Quinoxaline-Containing Polymers by Replacing Carbon with Silicon Bridging Atoms on Dithiophene Donor Skeleton

Xiaopeng Xu, Kai Li, Zuoja Li, Ying Li,* Zhenguo Wang, Qiang Peng*



Bridging atom effect shows great influence on thermal stability, the absorption, energy levels, carrier mobility and photovoltaic performance of Fluorinated quinoxaline-dithiophene based low band gap copolymers.